Letter

Splitting of nonequilibrium phase transitions in driven Ising models

Gustavo A. L. Forão,[1] Fernando S. Filho,[1,2] André P. Vieira,[1] Bart Cleuren,[2] Daniel M. Busiello,[3,4] and Carlos E. Fiore[1,*]

[1]Universidade de São Paulo, Instituto de Física, Rua do Matão, 1371, 05508-090 São Paulo, SP, Brazil
[2]UHasselt, Faculty of Sciences, Theory Lab, Agoralaan, 3590 Diepenbeek, Belgium
[3]Max Planck Institute for the Physics of Complex Systems, 01187 Dresden, Germany
[4]Department of Physics and Astronomy, University of Padova, 35131 Padova, Italy

(Received 19 December 2024; revised 13 May 2025; accepted 29 July 2025; published 4 September 2025)

Spontaneous symmetry breaking occurs in various equilibrium and nonequilibrium systems, where phase transitions are typically marked by a single critical point that separates ordered and disordered regimes. We reveal an innovative phenomenon in which the interplay between different temperatures and driving forces splits the order-disorder transition into two distinct transition points depending on which ordered state initially dominates. Crucially, these two emerging phases have distinct scaling behaviors and thermodynamic properties. To study this, we propose a minimal variant of the Ising model where spins are coupled to two thermal baths and subjected to two opposite driving forces associated with them. Our findings, robust for both all-to-all interactions (where exact solutions are possible) and nearest-neighbor couplings on a square lattice, uncover unique nonequilibrium behaviors and scaling laws for crucial thermodynamic quantities, such as efficiency, dissipation, power and its fluctuations, that are different between the two ordered phases. We also highlight that one of these emerging phases enables heat-engine operations that are less dissipative and show reduced fluctuations. In this setup, the system can also operate near maximum power and maximum efficiency over a wide parameter range. Our results offer unique insights into the relevance of phase transitions under nonequilibrium conditions.

DOI: 10.1103/hzl3-hjnl

Introduction. Phase transitions and universal scaling are central topics in statistical physics, particularly for systems that display collective behavior. Examples can be found across diverse fields, including physics, chemistry, biology, and economics. Many of these systems operate out of equilibrium, where nonzero probability currents and specific symmetries can lead to unique classes of nonequilibrium phase transitions. Similar to their equilibrium counterparts, nonequilibrium phase transitions are often characterized by an order parameter. However, this approach can obscure the irreversible dynamics and its impact on the properties of phase transitions. Increasing attention has been given to entropy production—a key indicator of system dissipation—and related thermodynamic quantities as alternative descriptors of nonequilibrium phase transitions, although many aspects of this topic remain to be understood [1–4].

Beyond phase transitions and universality classes, systems exhibiting collective dynamics are of considerable interest for their potential to enhance the performance of nonequilibrium heat engines, in both classical [5–12] and quantum thermodynamics [10,13,14]. A key subset of collective-engine setups extract work from driving forces, often modeled as biases over specific transitions [5–8,15,16]. These biases arise in diverse systems, such as anomalous mobility in driven active particles [17,18], chemical potentials fueling kinesin motion [19,20], light-activated transitions in photoacids [21], thermodynamic forces in chemical reaction networks [22–24], and ATP-driven pathways in chaperones and molecular transporters [25,26]. Recent studies highlight a distinct phase transition that separates a functional heat-engine regime from a "dud" regime, where the system is purely dissipative [7,8,15,16]. Despite its relevance in biophysics and related fields, the interplay between biased forces and phase transition regimes remains poorly understood and explored only in a few examples.

In this Letter, we demonstrate that collective effects under driving forces yield unique phenomena with no analog in traditional equilibrium or nonequilibrium phase transitions. The uniqueness lies in the combination of the following features: (1) Order-disorder phase transitions occur at separate points depending on which ordered phase initially dominates; (2) each order-disorder phase transition may fall into a different classification, with, for instance, the "down"-spin-dominated phase transition being critical and continuous, while the "up"-spin-dominated transition is discontinuous; and (3) unlike customary "up-down" (Z_2) symmetry-breaking phenomena [2,27], the continuous phase transition we observe exhibits critical exponents that, in the mean-field limit, differ from the classical result of $\beta = 1/2$. Our findings reveal different insights into the properties of the order parameter and uncover unique behaviors of key thermodynamic quantities, such as power and energy dissipation. We further show that the less dissipative ordered phase—characterized by lower power fluctuations—exhibits heat-engine behavior capable of

*Contact author: fiorecarlos.cf@gmail.com

achieving near-optimal efficiency and maximum power. In contrast to some recent studies [28–30], our results suggest that these performance improvements arise directly from collective dynamics, without the need for complex strategies.

Minimal collective model and thermodynamics. To illustrate these findings, we propose a minimal model consisting of N interacting units, where each unit j is represented by a spin variable s_j with values $s_j \in \{-1, 0, 1\}$. Thus, a given microscopic state is defined by the configuration of individual spins, $s \equiv (s_1, \ldots, s_j, \ldots, s_N)$. The energy of the system takes the simple Ising-like form

$$E(s) = \frac{\epsilon}{2k} \sum_{(i,j)} s_i s_j + \Delta \sum_{i=1}^{N} s_i^2, \tag{1}$$

where $\epsilon < 0$ quantifies the interaction energy between two nearest-neighbor units, and each unit contributes an individual energy 0 or Δ. The equilibrium version of this model exhibits a variety of collective behaviors, including continuous and discontinuous transitions, as well as tricritical points [31].

The system is coupled simultaneously to two thermal baths at different inverse temperatures β_1 and β_2 and inducing opposite nonconservative (biased) driving forces [5,7,15,19–21] acting at the level of individual units. Each step of the dynamics corresponds to flipping the state of a single unit (say unit j), under the action of one of the baths (with equal *a priori* probability), so that a microstate s is taken to $s' \equiv (s_1, \ldots, s_{j-1}, \tilde{s}_j, s_{j+1}, \ldots, s_N)$, where $\tilde{s}_j \neq s_j$. For a flip induced by bath $\nu \in \{1, 2\}$, the associated work performed on the system by the nonconservative force is

$$W_{s's}^{(\nu)} = (-1)^{\nu-1} d_{s's} F, \tag{2}$$

where F denotes the driving force strength and $d_{s's}$ equals $+1$ (-1) if the flip $s_j \to \tilde{s}_j$ follows clockwise (counterclockwise) the cycle $-1 \to 0 \to +1 \to -1$. Therefore, taking F to be positive, the cold thermal bath ($\nu = 1$) favors clockwise flips, while the hot bath ($\nu = 2$) favors counterclockwise flips (see also Fig. S1 in the Supplemental Material [32]). Notice that we adopt the convention that positive work is performed on the system, while work performed by the system is negative. Energy conservation implies that the associated heat is

$$Q_{s's}^{(\nu)} = E(s') - E(s) - W_{s's}^{(\nu)}. \tag{3}$$

The corresponding transition rate is $\omega_{s's}^{(\nu)} = \Gamma \exp[-(\beta_\nu/2) Q_{s's}^{(\nu)}]$, in which Γ sets the timescale. We should mention that the proposed dynamics is equivalent to the fast-switching limit of a "two-box" description [23,33,34] in which each unit is placed in contact with a single thermal bath at a time and a switching between thermal baths (while the unit is kept at the same state) occurs with a rate much greater than all other relevant rates.

The time evolution of the probability $p_s(t)$ to observe the system in the microstate s at time t is governed by the master equation

$$\dot{p}_s(t) = \sum_{\nu=1}^{2} \sum_{s' \neq s} J_{s's}^{(\nu)}(t), \tag{4}$$

where $J_{s's}^{(\nu)}(t) = \omega_{ss'}^{(\nu)} p_{s'}(t) - \omega_{s's}^{(\nu)} p_s(t)$ is the probability flux between microstates s and s' due to the contact with bath ν. We are mainly interested in the nonequilibrium steady-state (NESS) regime, in which the probability set $\{p_s^{\rm st}\}$ is time-independent.

Following Refs. [35,36], the mean heat exchange rate with each bath and the mean power are written as

$$\langle \dot{Q}_\nu \rangle = \sum_{(s,s')} Q_{s's}^{(\nu)} J_{s's}^{(\nu)} \quad \text{and} \quad \langle \mathcal{P} \rangle = \sum_{(s,s')} W_{s's}^{(\nu)} J_{s's}^{(\nu)}, \tag{5}$$

where sums over (s, s') involve all possible microstate flips. The above definitions satisfy the first and second laws of thermodynamics, respectively, $\langle \mathcal{P} \rangle + \langle \dot{Q}_1 \rangle + \langle \dot{Q}_2 \rangle = 0$ and $\langle \sigma \rangle = -\beta_1 \langle \dot{Q}_1 \rangle - \beta_2 \langle \dot{Q}_2 \rangle \geqslant 0$, where $\langle \sigma \rangle$ is the dissipation rate (or rate of entropy production), both evaluated in the NESS. A positive steady-state power indicates that, on average, work is performed on the system. In the opposite case of a negative steady-state power, the system operates, on average, as an engine, partially converting heat extracted from the hot reservoir into work.

In the nonequilibrium model, interactions give rise to collective effects, where phase transitions emerging as parameters (e.g., ϵ or Δ) are varied. Similar to the equilibrium model, two phases exist, denoted as A and B, respectively, characterized by a predominance of spins -1 and $+1$. Letting $m = -\langle s_i \rangle$ denote the order parameter, we have $m > 0$ for phase A and $m < 0$ for phase B, while $m = 0$ indicates independent operation of units. The "quadrupole moment" $q = \langle s_i^2 \rangle$ distinguishes between phases where units predominantly occupy states ± 1 ($q \approx 1$) and where they are in state 0 ($q = 0$).

Emergence of phase transitions with no equilibrium or nonequilibrium analogs. The interplay between biased driving forces and different ordered phases results in unique features of phase transitions with no equilibrium analog. Each ordered phase is associated with a distinct transition point, X_A or X_B (X being either ϵ or Δ) for $m > 0$ and $m < 0$, respectively, and, remarkably, these transitions can have different orders, with one being continuous and the other discontinuous [see Fig. 1(a)]. This contrasts with typical phase transitions characterized by spontaneous symmetry breaking, where the splitting of a transition point associated with hysteresis involves transitions that are *both* discontinuous, and that are related to stability limits of the ordered and disordered phases. To illustrate these features, we analyze interactions on both square-lattice arrangements (coordination number $k = 4$) and the all-to-all version ($k = N \to \infty$), the latter case yielding exact results that we now describe.

Following previous work [5–8,15], we describe the all-to-all dynamics via the densities of units in one of the possible individual states, $n_i = \langle N_i/N \rangle$, with $i \in \{-, 0, +\}$. Here, $N_\pm$ represents the number of units in the local states $s = \pm 1$ and N_0 is the number of units for which $s = 0$. The dynamics of $\{n_i\}$ is governed by the master equation

$$\dot{n}_i(t) = \sum_{\nu=1}^{2} \sum_{j \neq i} J_{ij}^{(\nu)}(t), \tag{6}$$

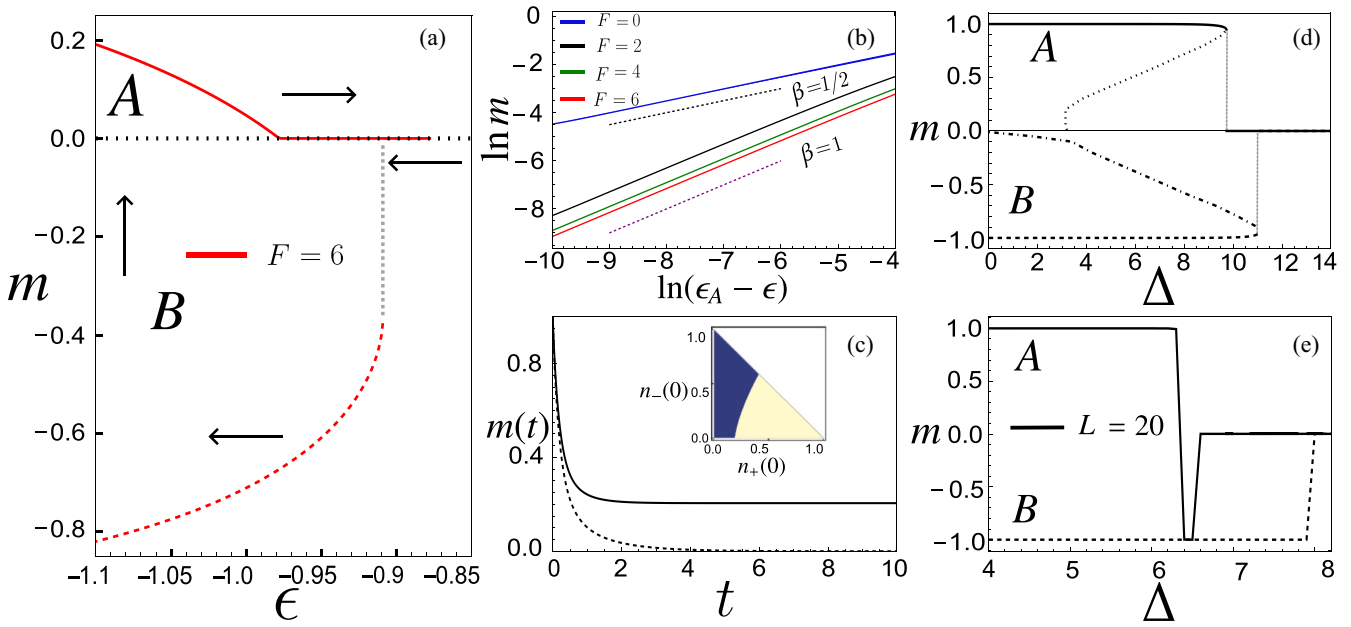

FIG. 1. (a) For all-to-all interactions and $\Delta = 0$, the figure shows the hysteresis involving the stationary values of the order parameter. The analysis starts with the system constrained to phase A by a very small magnetic field, at $\epsilon = \epsilon_0 = -1.1$. The parameter ϵ is increased quasistatically up to $\epsilon = -0.88$, past the (continuous) phase transition to the disordered phase occurring at $\epsilon = \epsilon_A = -0.978\,071$. Next, with the system in the disordered phase, the weak field is reversed, and the system is driven in the "backward" trajectory, in which the parameter ϵ is decreased quasistatically down to $\epsilon = \epsilon_0$, with the discontinuous phase transition to phase B occurring at $\epsilon = \epsilon_B = -0.908\,883$. Finally, the transition from phase B to phase A is achieved by applying an appropriate magnetic field at $\epsilon = \epsilon_0$. (b) Critical behavior associated with the ordered phase A, highlighting the difference between the $F = 0$ and the $F \neq 0$ cases. (c) Bistability of the magnetization close to the transition from the ordered phase B to the disordered phase, for $\epsilon = -0.9219$. Initial conditions are $n_+(0) = 0.8$, $n_-(0) = 0.2$ (solid line) and $n_+(0) = 0.2$, $n_-(0) = 0.8$ (dotted line). The inset shows the basins of attraction of the ordered (yellow area) and disordered (blue area) phases according to the values of $n_+(0)$ and $n_-(0)$. (d) Behavior of the order parameter as a function of Δ at fixed $\epsilon = -13$ for the all-to-all case. Dotted and dot-dashed lines denote the unstable solutions for the phases A and B, respectively. For phase A (B), initial conditions $m(0)$ lying above (below) the unstable solution will converge to the ordered solution. Otherwise, the disordered stationary solution will be reached. (e) Behavior of the order parameter as a function of Δ at fixed $\epsilon = -13$ for the square-lattice topology. The sudden jump from $m \approx 1$ to $m \approx -1$ is due to finite-size effects. Unless stated otherwise, parameters are $F = 2$, $\beta_1 = 2$, and $\beta_2 = 1$.

where $J_{ij}^{(\nu)}(t) = \omega_{ij}^{(\nu)} n_j(t) - \omega_{ji}^{(\nu)} n_i(t)$, with density-dependent transition rates $\omega_{ji}^{(\nu)}$ whose explicit expression is presented in the Supplemental Material. The order parameter m and the quadrupole moment q are given by $m = n_- - n_+$ and $q = n_- + n_+$. In the absence of individual energies ($\Delta = 0$), and for $|\beta_\nu \epsilon| \gg 1$, the steady state of the system corresponds to one of the two different ordered phases (A or B), depending on the initial condition. At fixed β_1 and β_2, by taking $X = \epsilon$ as the control parameter, as $\epsilon < 0$ increases the phase transition from phase A (B) to the disordered phase occurs at ϵ_A (ϵ_B), with $\epsilon_A < \epsilon_B < 0$. On the other hand, for $\epsilon > \epsilon_B$, the system is in the disordered phase, for which steady-state densities are equal, $n_+^{\rm st} = n_-^{\rm st} = n_0^{\rm st} = 1/3$, yielding $m = 0$ and $q = 2/3$. Finally, in the intermediate case $\epsilon_A < \epsilon < \epsilon_B$, the dynamics evolves to the disordered phase or to phase B, depending on the initial condition.

In order to analyze these phase transitions, we notice that, by combining the master equations for n_- and n_+, it is possible to derive master equations for m and q. In the steady state, $dm/dt = dq/dt = 0$, from which an implicit relation $q = q(m)$ can be obtained.

If there is a continuous phase transition to the disordered phase, the NESS values (m, q) continuously approach $(0, 2/3)$ as $\epsilon < 0$ is increased from the ordered phase at fixed β_1 and β_2. Therefore, it is possible to expand the master equation for dm/dt in m and, taking into account the implicit relation $q(m)$, the time evolution of m reads

$$\frac{dm}{dt} \approx a(\epsilon - \epsilon_A)m + bm^2 + cm^3 + \cdots, \tag{7}$$

where ϵ_A is given by

$$\epsilon_A = -\frac{e^{(1/2)F(\beta_1-\beta_2)} + e^{(1/2)F(\beta_2-\beta_1)} + e^{(1/2)F(\beta_1+\beta_2)} + e^{\beta_1 F} + e^{\beta_2 F} + 1}{(e^{\beta_1 F/2} + e^{\beta_2 F/2})(\beta_1 \cosh(\beta_1 F/2) + \beta_2 \cosh(\beta_2 F/2))},$$

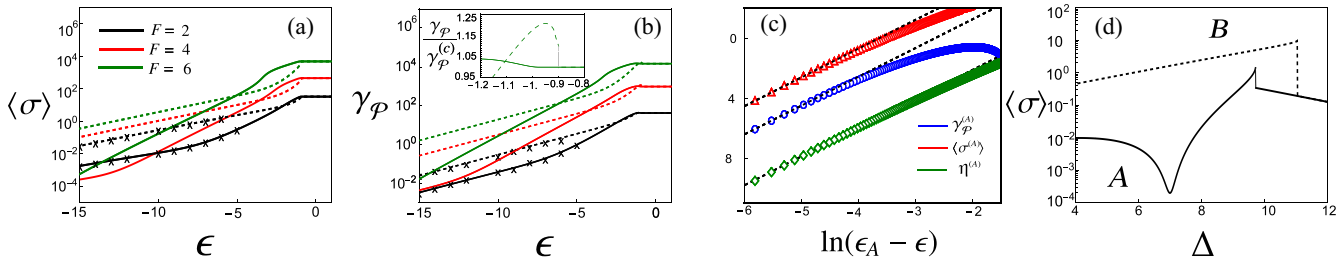

FIG. 2. (a) Average entropy production as a function of ϵ in phases A (solid lines) and B (dashed lines). (b) Same as panel (a) but for power fluctuations. The inset provides a close-up of $\gamma_{\mathcal{P}}$ near the phase transitions (dashed line indicates phase B). These findings are robust beyond the all-to-all interaction case, holding also for square-lattice interactions (data marked by $\times$). (c) Log-log plots of the above quantities near the critical point ϵ_A, with slopes consistent with $\delta = 2$. (d) Entropy production as a function of Δ for the same parameters as in Fig. 1 for phases A (solid line) and B (dashed line). As in Fig. 1(d), discontinuities occur at $\Delta_A = 9.73$ and $\Delta_B = 11.06$, respectively.

while

$$b = \sinh\left(\frac{F}{4}(\beta_1 - \beta_2)\right) f(\beta_1, \beta_2, F),$$

with explicit expressions for $f(\beta_1, \beta_2, F)$ and the coefficients $a > 0$ and c provided in the Supplemental Material.

A few observations about Eq. (7) are in order. First, the presence of a term proportional to m^2 for $F \neq 0$ and $\beta_1 \neq \beta_2$ leads to the critical behavior $m \sim a(\epsilon_A - \epsilon)/b$, with a critical exponent $\beta = 1$ (not to be confused with the inverse bath temperatures β_1 and β_2), markedly different from the standard mean-field behavior in order-disorder phase transitions $|m| \sim \sqrt{a(\epsilon_A - \epsilon)/c}$, where $\beta = 1/2$, obtained when $F = 0$ and/or $\beta_1 = \beta_2$. The appearance of a critical exponent $\beta = 1$, illustrated in Fig. 1(b), is a consequence of breaking the Z_2-"up-down" symmetry that is often present in equilibrium and nonequilibrium phase transitions for mean-field systems [2,3]. Two additional distinctions from standard order-disorder phase transitions are that $\epsilon_B \neq \epsilon_A$ and, for $\Delta = 0$, the classifications of the corresponding phase transitions differ. While the transition from $m > 0$ to the disordered phase is continuous, the one from $m < 0$ is discontinuous, as shown in Fig. 1(a). Unlike a critical transition, the latter case features a spinodal region where the system may reach two distinct steady states depending on the initial configuration [see Fig. 1(c)]. This behavior remains qualitatively the same as long as $F \neq 0$. In the absence of the nonconservative force, the splitting of the phase transitions disappears.

The existence of two distinct transition points is robust, as shown in Figs. 1(d) and 1(e), where we fix the values of β_1, β_2, and ϵ while varying the individual-energy parameter Δ, both in the all-to-all case [Fig. 1(d)] and in the square lattice [Fig. 1(e)], the latter case having been studied by numerical simulations via the Gillespie algorithm [37]. Notice that now both transitions are discontinuous, with the jumps in the order parameter and the spinodal regions being more pronounced (dotted and dot-dashed lines) than for $\Delta = 0$. Notably, hints of a similar scenario have been observed in a simpler two-state model [7,15], where the $m > 0$ phase exhibits a discontinuous phase transition, absent for $m < 0$.

These findings are also reflected in peculiar thermodynamic properties of this class of systems. In the following, we analyze the average power $\langle \mathcal{P} \rangle$ and the power fluctuations $\gamma_{\mathcal{P}} \equiv \langle \mathcal{P}^2 \rangle - \langle \mathcal{P} \rangle^2$, the efficiency $\eta = -\langle \mathcal{P} \rangle / \langle \dot{Q}_2 \rangle$, and the dissipation $\langle \sigma \rangle$. We use the superscripts (A) and (B) to distinguish between quantities associated with phases A ($m > 0$) and B ($m < 0$).

In the all-to-all limit, by expanding $\langle \sigma^{(A)} \rangle$ and $\gamma_{\mathcal{P}}^{(A)}$ in terms of the order parameter near ϵ_A, we arrive at the following expressions:

$$\langle \sigma^{(A)} \rangle \sim \langle \sigma_c \rangle + c_\sigma m^2 + \cdots,$$
$$\gamma_{\mathcal{P}}^{(A)} \sim \gamma_{\mathcal{P}}^{(c)} + c_v m^2 + \cdots,$$

where $\langle \sigma_c \rangle = 2F[\beta_1 \sinh(\beta_1 F/2) + \beta_2 \sinh(\beta_2 F/2)]$ and $\gamma_{\mathcal{P}}^{(c)} = 2F^2[\cosh(\beta_1 F/2) + \cosh(\beta_2 F/2)]$, respectively, denote entropy production and power variance for $\epsilon \geqslant \epsilon_A$. The coefficients c_σ and c_v are provided in the Supplemental Material. This dependence on the order parameter implies another scaling behavior, i.e., $\langle \sigma^{(A)} \rangle - \langle \sigma_c \rangle \sim a c_\sigma (\epsilon_A - \epsilon)^\delta / b$ and $\gamma_{\mathcal{P}}^{(A)} - \gamma_{\mathcal{P}}^{2(c)} \sim a c_v (\epsilon_A - \epsilon)^\delta / b$, with $\delta = 2\beta = 2$. Average entropy production and power fluctuations as functions of ϵ are shown in Figs. 2(a) and 2(b).

The system's performance, particularly its efficiency η, also has a scaling behavior characterizing phase A. To examine this, we expand $\langle \dot{Q}_i^{(A)} \rangle$ around ϵ_A, yielding $\langle \dot{Q}_i^{(A)} \rangle \sim \langle \dot{Q}_i^{(c)} \rangle + c_{q_i} m^2 + \cdots$, where $\langle \dot{Q}_i^{(c)} \rangle = -2F \sinh(\beta_i F/2)$ and the coefficients c_{q_1} and c_{q_2} are listed in the Supplemental Material. Using the expressions for $\langle \dot{Q}_2^{(A)} \rangle$ and $\langle \mathcal{P}^{(A)} \rangle$, we derive an asymptotic form of the efficiency $\eta^{(A)}$,

$$\eta^{(A)} \sim \eta^{(c)} + \frac{1}{\langle \dot{Q}_2^{(c)} \rangle} \left(c_{q_1} - \frac{c_{q_2} \langle \dot{Q}_1^{(c)} \rangle}{\langle \dot{Q}_2^{(c)} \rangle} \right) (\epsilon_A - \epsilon)^\delta,$$

where $\eta^{(c)} = 1 + \sinh(\beta_1 F/2)/\sinh(\beta_2 F/2)$ and $\delta = 2\beta$. Thus, the efficiency exhibits the same critical exponent as entropy production, power, and power fluctuations, as illustrated in Fig. 2(c). Although closed-form expressions are unavailable near ϵ_B, Fig. 2(b) (dashed line in the inset) shows that the discontinuity in the order parameter can be equally found in power fluctuations $\gamma_{\mathcal{P}}$. Moreover, when analyzing the system in the ordered phases, we notice that phase A ($m > 0$) exhibits notably lower dissipation and power fluctuations than phase B ($m < 0$), as shown in Figs. 2(a) and 2(b).

To gain more intuition on the system's behavior, we develop a phenomenological model valid when $|m| \approx 1$, using an approach analogous to that introduced in Ref. [7]. Under this condition, the state densities are approximately given by $n_- = 1$ ($n_- = 0$) and $n_+ = 0$ ($n_+ = 1$) for phase A (B).

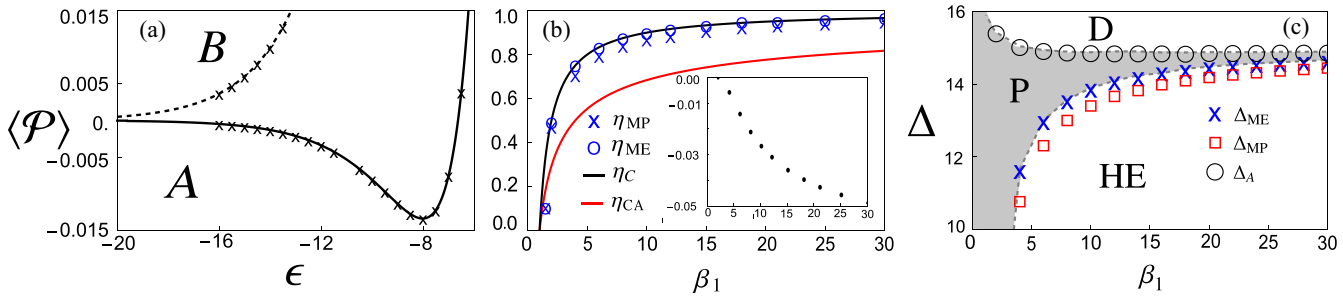

FIG. 3. (a) Average power $\langle \mathcal{P} \rangle$ as a function of ϵ in phases A (solid line) and B (dashed line) for the same parameters as in Fig. 1. Symbols indicate the square-lattice case. (b) $\eta_{\rm MP}$ (symbols $\times$) and $\eta_{\rm ME}$ (symbols $\circ$) versus β_1 for $\epsilon = -20$ and $F = 5$. For comparison, the continuous black and red curves represent the corresponding Carnot η_c and the Curzon-Ahlborn efficiency $\eta_{\rm CA}$, respectively. The inset shows the corresponding maximum power values, $\mathcal{P}_{\rm MP}$. (c) The convergence of $\Delta_{\rm MP}$ and $\Delta_{\rm ME}$ to Δ_A is shown, as a function of β_1 for the same parameters as in panel (b). Dashed curves here separate the heat-engine (HE) and dud (D) regimes from the heat pump behavior (gray area). In all cases, $\beta_2 = 1$.

Applying the spanning-tree method [38], we derive approximate steady-state solutions, depending only on model parameters (details in the Supplemental Material). For $|\beta_\nu(\epsilon + \Delta)| \gg 1$, the effective expressions for the entropy production are given by

$$\langle \sigma_{\rm eff}^{(A)} \rangle \approx -e^{(1/2)\beta_2(\Delta - F + \epsilon)}[F(\beta_1 + \beta_2) + (\beta_1 - \beta_2)(\Delta + \epsilon)]$$

and

$$\langle \sigma_{\rm eff}^{(B)} \rangle \approx e^{(\beta_2/2)(\Delta + F + \epsilon)}[F(\beta_1 + \beta_2) - (\beta_1 - \beta_2)(\Delta + \epsilon)]$$

for phases A and B, respectively. Notice that $0 < \langle \sigma_{\rm eff}^{(A)} \rangle < \langle \sigma_{\rm eff}^{(B)} \rangle$. Similarly, expressions for the power fluctuations $\gamma_{\mathcal{P}}$ are obtained via the large-deviation method [39,40], with leading terms given by $\gamma_{\mathcal{P}}^{(A)} \approx 4F^2[e^{(\beta_1/2)(\epsilon+F)} + e^{(\beta_2/2)(\epsilon-F)}]$ and $\gamma_{\mathcal{P}}^{(B)} \approx 4F^2 e^{(\beta_2/2)(\epsilon+F)}$ for phases A and B, respectively. Here again, $\gamma_{\mathcal{P}}^{(A)} < \gamma_{\mathcal{P}}^{(B)}$, consistent with phase A exhibiting lower power fluctuations than phase B. These results are also valid in the square-lattice topology [see data marked by the symbols $\times$ in Figs. 2(a) and 2(b)].

Also, in Fig. 2(d), we show the behavior of $\langle \sigma \rangle$ in the square lattice as Δ varies. Again, $\langle \sigma^{(A)} \rangle$ (solid lines) remains smaller than $\langle \sigma^{(B)} \rangle$ (dashed lines). The entropy production, like the order parameter, captures again the phase transitions occurring at two distinct values of Δ, $\Delta_A \neq \Delta_B$.

Phase transitions and heat engines operating on the verge of maximum power and maximum efficiency. Systems operating collectively can offer significant advantages, such as reducing dissipated work [12,41] and optimizing efficiency and/or power through tailored internal structures [7,11,15]. Here, we notice a crucial difference in behavior emerging from the existence of the two phases. Indeed, assuming $F > 0$, the system may only operate as a heat engine for $m > 0$ (phase A) and not for $m < 0$ (phase B), as illustrated in Fig. 3(a). The engine regime occurs deep in the ordered phase with $m \approx 1$, in which case the majority of units are in the state $s_j = -1$. Due to the values of the transition amplitudes, only rarely a unit flips, mostly to $s_j = 0$, under the action of the hot bath, flipping back to $s_j = -1$ under the action of the cold bath. Both flips involve performing work on the surroundings. On the other hand, if $m \approx -1$, the most common excitation involves flips from the state $s_j = +1$ to $s_j = 0$ under the action of the hot bath, flipping back to $s_j = +1$ under the action of the cold bath. Both flips now involve work performed on the system. (If $F < 0$, the roles of the A and B phases are interchanged.)

The phenomenological description employed above allows the quantification of this effect via expressions for $\langle \mathcal{P} \rangle$ and η. When $|\beta_\nu(\epsilon + \Delta)| \gg 1$ and β_1 is sufficiently different from β_2 so that the system can operate as a heat engine, these quantities read

$$\langle \mathcal{P}_{\rm eff}^{(A)} \rangle = \frac{2F\left(e^{\frac{1}{2}\beta_1(\Delta+\epsilon+F)} - e^{\frac{1}{2}\beta_2(\Delta+\epsilon-F)}\right)}{e^{\frac{1}{2}((\beta_1+\beta_2)(\Delta+\epsilon)+F(\beta_1-\beta_2))} + 1} \tag{8}$$

and

$$\eta_{\rm eff}^{(A)} = \frac{2F}{F - \epsilon - \Delta}\left(e^{\frac{1}{2}\{(\beta_1+\beta_2)(\Delta+\epsilon)+F(\beta_1-\beta_2)\}} + 1\right), \tag{9}$$

for phase A. Similar expressions for phase B show that $\langle \mathcal{P}_{\rm eff}^{(B)} \rangle > 0$ and $\eta_{\rm eff}^{(B)} < 0$, so that, in this phase, the system never operates as a heat engine. On the other hand, for sufficiently distinct values of β_1 and β_2, there is a range of values of β_1 in which the system, in phase A, operates as a heat engine close to maximum power and maximum efficiency, as shown in Fig. 3(b) and in the Supplemental Material. While the second law of thermodynamics prevents ideal efficiency at finite power, the interactions and individual-energy distributions allow for the maximization of power and efficiency at values of Δ denoted by $\Delta_{\rm MP}$ and $\Delta_{\rm ME}$, respectively, with the other parameters held fixed. These values are close to each other, enabling near-ideal performance (i.e., near maximum power and efficiency). They converge toward the ideal efficiency $\eta_c = 1 - \beta_2/\beta_1$ as β_1 increases. These findings hold not only for all-to-all interactions but also in square-lattice configurations [marked by $\times$ symbols in Fig. 3(a)], without requiring specialized optimization procedures, such as reward functions that balance power and efficiency.

Finally, we address the link between optimization and phase transitions. Although $\Delta_{\rm MP}$ and $\Delta_{\rm ME}$ do not necessarily coincide, both converge to the discontinuous transition value $\Delta = \Delta_A$ as β_1 increases [see Fig. 3(c)], revealing a connection between ideal operational conditions and phase transitions.

Conclusions. Our results reveal a class of collective behaviors under driven forces, with a unique phase transition characterized by two distinct transition points. These findings highlight the emergence of ordered phases with

contrasting behaviors, where phase *A*, the less dissipative phase, exhibits weaker power fluctuations and supports nearly ideal performance under optimal energy settings. Our work opens avenues for a deeper understanding of sheer nonequilibrium phenomena driving collective operation and instantiating efficient heat engines at the nanoscale. Future investigations could explore more complex systems, such as those with energetic frustration, which frequently appear in nature and could yield further insights into this field.

Acknowledgments. We acknowledge the financial support from Brazilian agencies CNPq 309311/2021-7 and 300244/2025-8 and FAPESP under Grants No. 2021/03372-2, No. 2022/16192-5, No. 2022/15453-0, No. 2023/12490-4, No. 146224/2021-3, and No. 2024/03763-0. F.S.F. was also supported by the Special Research Fund (BOF) of UHasselt (BOF23DOCBL14).

Data availability. No data were created or analyzed in this study.

[1] T. Tomé and M. J. de Oliveira, Entropy production in nonequilibrium systems at stationary states, Phys. Rev. Lett. **108**, 020601 (2012).

[2] C. E. F. Noa, P. E. Harunari, M. J. de Oliveira, and C. E. Fiore, Entropy production as a tool for characterizing nonequilibrium phase transitions, Phys. Rev. E **100**, 012104 (2019).

[3] M. Aguilera, M. Igarashi, and H. Shimazaki, Nonequilibrium thermodynamics of the asymmetric Sherrington-Kirkpatrick model, Nat. Commun. **14**, 3685 (2023).

[4] S. A. Loos, S. H. Klapp, and T. Martynec, Long-range order and directional defect propagation in the nonreciprocal *XY* model with vision cone interactions, Phys. Rev. Lett. **130**, 198301 (2023).

[5] T. Herpich, J. Thingna, and M. Esposito, Collective power: Minimal model for thermodynamics of nonequilibrium phase transitions, Phys. Rev. X **8**, 031056 (2018).

[6] T. Herpich and M. Esposito, Universality in driven Potts models, Phys. Rev. E **99**, 022135 (2019).

[7] F. S. Filho, G. A. L. Forão, D. M. Busiello, B. Cleuren, and C. E. Fiore, Powerful ordered collective heat engines, Phys. Rev. Res. **5**, 043067 (2023).

[8] I. N. Mamede, K. Proesmans, and C. E. Fiore, Thermodynamics of interacting systems: The role of the topology and collective effects, Phys. Rev. Res. **5**, 043278 (2023).

[9] C. G. Feyisa and H. H. Jen, Trapped-atom Otto engine with light-induced dipole–dipole interactions, New J. Phys. **26**, 093039 (2024).

[10] L. P. Bettmann, M. J. Kewming, and J. Goold, Thermodynamics of a continuously monitored double-quantum-dot heat engine in the repeated interactions framework, Phys. Rev. E **107**, 044102 (2023).

[11] S. Liang, Y.-H. Ma, D. M. Busiello, and P. De Los Rios, Minimal model for Carnot efficiency at maximum power, Phys. Rev. Lett. **134**, 027101 (2025).

[12] A. Rolandi, P. Abiuso, and M. Perarnau-Llobet, Collective advantages in finite-time thermodynamics, Phys. Rev. Lett. **131**, 210401 (2023).

[13] M. Campisi and R. Fazio, The power of a critical heat engine, Nat. Commun. **7**, 11895 (2016).

[14] L. da SilvaSouza, G. Manzano, R. Fazio, and F. Iemini, Collective effects on the performance and stability of quantum heat engines, Phys. Rev. E **106**, 014143 (2022).

[15] H. Vroylandt, M. Esposito, and G. Verley, Collective effects enhancing power and efficiency, Europhys. Lett. **120**, 30009 (2017).

[16] H. Vroylandt, M. Esposito, and G. Verley, Efficiency fluctuations of stochastic machines undergoing a phase transition, Phys. Rev. Lett. **124**, 250603 (2020).

[17] R. N. Valani, Anomalous transport of a classical wave-particle entity in a tilted potential, Phys. Rev. E **105**, L012101 (2022).

[18] R. N. Valani and B. S. Dandogbessi, Asymmetric limit cycles within Lorenz chaos induce anomalous mobility for a memory-driven active particle, Phys. Rev. E **110**, L052203 (2024).

[19] S. Liepelt and R. Lipowsky, Kinesin's network of chemomechanical motor cycles, Phys. Rev. Lett. **98**, 258102 (2007).

[20] S. Liepelt and R. Lipowsky, Operation modes of the molecular motor kinesin, Phys. Rev. E **79**, 011917 (2009).

[21] C. Berton, D. M. Busiello, S. Zamuner, E. Solari, R. Scopelliti, F. Fadaei-Tirani, K. Severin, and C. Pezzato, Thermodynamics and kinetics of protonated merocyanine photoacids in water, Chem. Sci. **11**, 8457 (2020).

[22] S. Liang, P. De Los Rios, and D. M. Busiello, Thermodynamic bounds on symmetry breaking in linear and catalytic biochemical systems, Phys. Rev. Lett. **132**, 228402 (2024).

[23] D. M. Busiello, S. Liang, F. Piazza, and P. De Los Rios, Dissipation-driven selection of states in non-equilibrium chemical networks, Commun. Chem. **4**, 16 (2021).

[24] R. Rao and M. Esposito, Nonequilibrium thermodynamics of chemical reaction networks: Wisdom from stochastic thermodynamics, Phys. Rev. X **6**, 041064 (2016).

[25] P. De Los Rios and A. Barducci, Hsp70 chaperones are non-equilibrium machines that achieve ultra-affinity by energy consumption, elife **3**, e02218 (2014).

[26] S. Flatt, D. M. Busiello, S. Zamuner, and P. De Los Rios, ABC transporters are billion-year-old Maxwell demons, Commun. Phys. **6**, 205 (2023).

[27] M. Aguilera, S. A. Moosavi, and H. Shimazaki, A unifying framework for mean-field theories of asymmetric kinetic Ising systems, Nat. Commun. **12**, 1197 (2021).

[28] N. Pancotti, M. Scandi, M. T. Mitchison, and M. Perarnau-Llobet, Speed-ups to isothermality: Enhanced quantum thermal machines through control of the system-bath coupling, Phys. Rev. X **10**, 031015 (2020).

[29] P. A. Erdman and F. Noé, Model-free optimization of power/efficiency tradeoffs in quantum thermal machines using reinforcement learning, PNAS Nexus **2**, pgad248 (2023).

[30] P. A. Erdman, A. Rolandi, P. Abiuso, M. Perarnau-Llobet, and F. Noé, Pareto-optimal cycles for power, efficiency and fluctuations of quantum heat engines using reinforcement learning, Phys. Rev. Res. **5**, L022017 (2023).

[31] J. M. Yeomans, *Statistical Mechanics of Phase Transitions* (Clarendon Press, Oxford, 1992).

[32] See Supplemental Material at http://link.aps.org/supplemental/10.1103/hzl3-hjnl for more details about the model description, main expressions for thermodynamic quantities and heat-engines.

[33] D. M. Busiello, D. Gupta, and A. Maritan, Coarse-grained entropy production with multiple reservoirs: Unraveling the role of time scales and detailed balance in biology-inspired systems, Phys. Rev. Res. **2**, 043257 (2020).

[34] S. Liang, P. De Los Rios, and D. M. Busiello, Dissipation-driven selection under finite diffusion: Hints from equilibrium and separation of time scales, Entropy **23**, 1068 (2021).

[35] M. Esposito and C. Van den Broeck, Three faces of the second law. I. Master equation formulation, Phys. Rev. E **82**, 011143 (2010).

[36] C. Van den Broeck and M. Esposito, Ensemble and trajectory thermodynamics: A brief introduction, Physica A **418**, 6 (2015).

[37] D. T. Gillespie, Exact stochastic simulation of coupled chemical reactions, J. Phys. Chem. **81**, 2340 (1977).

[38] J. Schnakenberg, Network theory of microscopic and macroscopic behavior of master equation systems, Rev. Mod. Phys. **48**, 571 (1976).

[39] H. Touchette, The large deviation approach to statistical mechanics, Phys. Rep. **478**, 1 (2009).

[40] N. Kumar, C. Van den Broeck, M. Esposito, and K. Lindenberg, Thermodynamics of a stochastic twin elevator, Phys. Rev. E **84**, 051134 (2011).

[41] J. Meibohm and M. Esposito, Minimum-dissipation principle for synchronized stochastic oscillators far from equilibrium, Phys. Rev. E **110**, L042102 (2024).